Effects of Multiple Scattering on Light Pulses Reflected by Turbid Atmospheres

J. A. WEINMAN

Department of Meteorology, University of Wisconsin, Madison 53706

(Manuscript received 6 March 1975, in revised form 25 March 1976)

ABSTRACT

Multiple scattering contributions to lidar returns from turbid atmospheres are derived by means of an analytical theory. It is assumed that scattering takes place mainly at small angles except for one event that scatters the light backward. The phase functions are approximated by the sum of Gaussian functions of the scattering angle in both the forward and backward directions. The three-dimensional radiative transfer equation is transformed to a one-dimensional problem by means of Fourier transforms. Neumann solutions to the transformed equation of radiative transfer are then found. A number of examples are presented for cloud, fog and haze models. The results are found to be in satisfactory agreement with results obtained from the Monte Carlo analysis of Kunkel (1974) and the theory of light pulses doubly scattered by turbid atmospheres which was developed by Eloranta (1972).

1. Introduction

Pulses of light emitted by lasers which are reflected from particles in the atmosphere provide a technique to probe the optical properties and the spatial distribution of the particles. A receiver consisting of a telescope with a photomultiplier at the focus is frequently mounted alongside the laser transmitter to comprise a monostatic lidar system (see Derr, 1972). Optical properties of particles in the atmosphere can be determined by the analysis of the temporal variation of the scattered light flux measured by the receiver if the light has been scattered only once. However, the problem becomes more difficult to analyze if the particle density becomes sufficient so that light is multiply scattered before it is measured at the receiver.

The Monte Carlo method provides the most definitive analysis of the temporal variation of light pulses multiply scattered backward to a lidar receiver (see, e.g., Collins and Wells, 1965; Plass and Kattawar, 1971; Kunkel, 1974). Unfortunately solutions of the lidar problem by means of the Monte Carlo method are time consuming so that it is impractical to analyze lidar data from a variety of physical situations. Analytical solutions to this problem are required to conveniently analyze lidar data obtained in fogs, clouds or haze. The study of Rybicki (1971) provides useful guidance for the solution of this problem; however, it considers scattering from a medium composed of isotropically scattering particles, whereas clouds and hazes scatter anisotropically.

We now proceed to derive an approximate analytical expression for multiply scattered lidar returns from anisotropically scattering atmospheres.

2. Analysis

We will confine our attention to the lidar geometry shown in Fig. 1. The scattering medium will be assumed to be homogeneous.

Let the radiance I satisfy the time-dependent three-dimensional radiative transfer equation

$$\frac{1}{c}\frac{\partial I}{\partial t'}+\cos\theta\frac{\partial I}{\partial x'}+\sin\theta\cos\phi\frac{\partial I}{\partial y'}+\sin\theta\sin\phi\frac{\partial I}{\partial z'}+\beta I = \frac{\tilde{\omega}\beta}{4\pi}\int_0^{2\pi}\int_0^{\pi} I(t',x',y',z',\theta',\phi') \times P(\theta',\phi';\theta,\phi)\sin\theta' d\theta' d\phi', \quad (1)$$

where:

c	velocity of light
t'	time
x'	coordinate axis along direction of propagation
y', z'	coordinate axes perpendicular to axis of propagation
β	extinction coefficient
$\tilde{\omega}$	albedo for single scattering
θ	zenith angle
ϕ	azimuth angle
$P(\theta',\phi';\theta,\phi)$	phase function which describes scattering from (θ',ϕ') to (θ,ϕ).

The scattered radiance I originates as a narrow pulse in time and as a narrowly collimated beam at $x'=0$, *viz.*

$$I(x'=0)=\delta(t')\delta(y')\delta(z')\delta(\theta)\delta(\phi), \quad (2)$$

where $\delta(q)$ is Dirac's delta function.

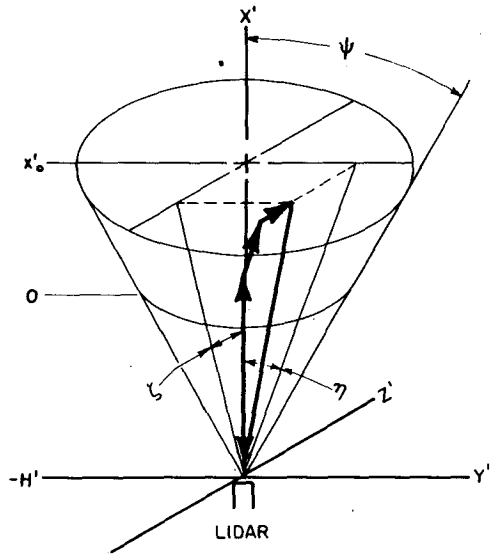

FIG. 1. Schematic view of geometry of the lidar problem.

The analysis which yields Eq. (21) of Weinman and Shipley's (1972) study shows that detours from the x' axis due to small-angle scattering cause delays of the order of

$$\delta t' \approx 0.033\beta x'^2/c\gamma \approx 3\times 10^{-8}\ \text{s}, \tag{3}$$

when the extinction coefficient is 10 km^{-1}, the thickness is 5 km, and γ is the reciprocal of the scattering angle variance for a narrow diffraction peak [see Eq. (7) of Weinman and Shipley (1972)]. Such delays are small compared to the transit time for laser pulses commonly found in turbid atmospheres. It is thus convenient to separate the time dependence from the space dependence of I, *viz.*

$$I(t',x',y',z',\theta,\phi) = \tilde{I}(x',y',z',\theta,\phi) f(x'-ct'). \tag{4}$$

By combining Eqs. (2) and (4) we obtain

$$I(t',x',y',z',\theta,\phi) = \tilde{I}(x',y',z',\theta,\phi)\delta(x'-ct'). \tag{5}$$

Radiances which are scattered by large angles, other than those near $\theta \approx \pi$, are considered to be rendered unavailable to the backscattered lidar signal. It is thus expedient to separate the radiance into parts which represent energy scattered at small angles, $\hat{I}$, and at large angles, $\bar{I}$:

$$\tilde{I}(x',y',z',\theta,\phi) = \hat{I}(x',y',z',\theta,\phi) + \bar{I}(x',y',z',\theta,\phi). \tag{6a}$$

The phase function may also be separated into small angle $\hat{P}$ and large angle $\bar{P}$ components, i.e.,

$$P(\theta',\phi';\theta,\phi) = \hat{P}(\theta',\phi';\theta,\phi) + \bar{P}(\theta',\phi';\theta,\phi). \tag{6b}$$

Subsequent considerations will be confined to the solution of those radiances scattered at small angles only, save for the one scattering event at $\theta \approx \pi$ which deflects the transmitted radiance back to the receiver. Thus, the part of Eq. (1) which governs small angle scattering is

$$\frac{\partial \hat{I}}{\partial x} + \eta\frac{\partial \hat{I}}{\partial y} + \zeta\frac{\partial \hat{I}}{\partial z} + \hat{I} = \frac{\tilde{\omega}}{4\pi}\int_{-\infty}^{\infty}\int_{-\infty}^{\infty} \hat{I}(x,y,z,\eta',\zeta')\hat{P}(\eta',\zeta';\eta,\zeta)d\eta' d\zeta', \tag{7}$$

where

$$\sin\theta \approx \theta, \quad \eta = \theta\cos\phi$$

$$\cos\theta \approx 1, \quad \zeta = \theta\sin\phi$$

$\Theta = [(\eta-\eta')^2 + (\zeta-\zeta')^2]^{\frac{1}{2}}$ is the scattering angle,

$$\frac{\hat{P}(\Theta)}{4\pi}\tilde{\omega} = \sum_{i=1}^{I}\frac{a_i\gamma_i}{\pi}\exp(-\gamma_i\Theta^2)$$

is a multi-Gaussian approximation to the phase function (see Weinman *et al.*, 1975), and x, y and z are coordinates in units of optical thickness $\beta x'$, $\beta y'$ and $\beta z'$, respectively.

We will now develop a Neumann solution which yields radiances which have been scattered successively. The Neumann solution for this problem is

$$\hat{I} = \sum_{m=1}^{\infty}\hat{I}_m, \tag{8}$$

where

$$\frac{\partial \hat{I}_m}{\partial x} + \eta\frac{\partial \hat{I}_m}{\partial y} + \zeta\frac{\partial \hat{I}_m}{\partial z} + \hat{I}_m = (1-\delta_{m,1})\sum_{i=1}^{I}\frac{a_i\gamma_i}{\pi} \times \int_{-\infty}^{\infty}\int_{-\infty}^{\infty}\exp\{-\gamma_i[(\eta-\eta')^2+(\zeta-\zeta')^2]\} \times \hat{I}_{m-1}(\eta',\zeta')d\eta' d\zeta', \tag{9}$$

where

$$\delta_{m,1} = \begin{cases} 1 & \text{if } m=1 \\ 0 & \text{if } m>1. \end{cases}$$

The complexity of the solution of Eq. (9) can be reduced if the transverse displacements of the multiply scattered radiances are first averaged rather than evaluated explicitly at each scattering event. The average squared displacement is

$$\langle y^2\rangle + \langle z^2\rangle = \sum_{k,l}[(x_0-x_k)(x_0-x_l)(\eta_k\eta_l+\zeta_k\zeta_l)] = \sum_{k}\langle(x_0-x_k)^2\rangle\Theta^2. \tag{10}$$

The right-hand expression is a consequence of azimuthal averaging which yields

$$\langle\cos\phi_k\cos\phi_l\rangle = \langle\sin\phi_k\sin\phi_l\rangle = \tfrac{1}{2}\delta_{k,l}, \tag{11}$$

where the Kronecker delta is defined in Eq. (9).

The squared scattering path is

$$\sum_k \langle (x_0-x_k)^2\rangle = \frac{1}{x_0}\int_0^{x_0}(x_0-x)^2dx = \frac{x_0^2}{3}. \quad (12)$$

Therefore, the average squared transverse displacement becomes

$$\langle y^2\rangle + \langle z^2\rangle = x_0^2\Theta^2/3, \quad (13)$$

which permits us to rewrite the differential operator of Eq. (9) for $m>1$ as

$$\frac{\partial \hat{I}_m}{\partial x}+\eta\frac{\partial \hat{I}_m}{\partial y}+\zeta\frac{\partial \hat{I}_m}{\partial z}\cong\frac{\partial \hat{I}_m}{\partial x}+\frac{\eta}{3^{\frac{1}{2}}}\frac{\partial \hat{I}_m}{\partial\langle y^2\rangle^{\frac{1}{2}}}+\frac{\zeta}{3^{\frac{1}{2}}}\frac{\partial \hat{I}_m}{\partial\langle z^2\rangle^{\frac{1}{2}}}. \quad (14)$$

Eqs. (9) and (14) can be solved analytically by taking two-dimensional Fourier transforms of $\hat{I}_m$, i.e.,

$$\hat{\imath}_1(x,p,q,\eta,\zeta)=\frac{1}{2\pi}\int_{-\infty}^{\infty}\int_{-\infty}^{\infty}\hat{I}_1(x,y,z,\eta,\zeta)\times\exp[j(py+qz)]dydz, \quad (15a)$$

$$\hat{\imath}_m(x,p,q,\eta,\zeta)=\frac{1}{2\pi}\int_{-\infty}^{\infty}\int_{-\infty}^{\infty}\hat{I}_m(x,\langle y^2\rangle^{\frac{1}{2}},\langle z^2\rangle^{\frac{1}{2}},\eta,\zeta)\times\exp[j(p\langle y^2\rangle^{\frac{1}{2}}+q\langle z^2\rangle^{\frac{1}{2}})]d\langle y^2\rangle^{\frac{1}{2}}d\langle z^2\rangle^{\frac{1}{2}}, \quad (15b)$$

for $m>1$ and where $j^2=-1$.

Eqs. (9 and 14) then become

$$\frac{\partial \hat{\imath}_1}{\partial x}+[1-j(\eta p+\zeta q)]\hat{\imath}_1=0, \quad (16a)$$

$$\frac{\partial \hat{\imath}_m}{\partial x}+[1-j(\eta p+\zeta q)/\sqrt{3}]\hat{\imath}_m=\sum_{i=1}^{I}\frac{a_i\gamma_i}{\pi}\int_{-\infty}^{\infty}\int_{-\infty}^{\infty}\exp\{-\gamma_i[(\eta-\eta')^2+(\zeta-\zeta')^2]\}\times\hat{\imath}_{m-1}(\eta',\zeta')d\eta'd\zeta', \quad m>1. \quad (16b)$$

Note that the effect of successive transverse displacements is only considered on the average with this representation.

The boundary condition which applies to the cloud base is

$$\hat{\imath}_1(0,p,q,\eta,\zeta)=\delta(\eta)\delta(\zeta)/2\pi. \quad (16c)$$

This is a one-dimensional Neumann radiative transfer problem similar to that investigated by Weinman *et al.* (1975); however, one must deal with a complex extinction coefficient in the present problem. It follows that

$$\hat{\imath}_1(x,p,q,\eta,\zeta)=\frac{\delta(\eta)\delta(\zeta)}{2\pi}\exp\{-[1-j(\eta p+\zeta q)]x\}, \quad (17a)$$

and for $m>1$

$$\hat{\imath}_m(x,p,q,\eta,\zeta)=\int_0^x \hat{J}_{m-1}(\tilde{x},p,q,\eta,\zeta)\times\exp\{-[1-j(\eta p+\zeta q)/\sqrt{3}][x-\tilde{x}]\}d\tilde{x}, \quad (17b)$$

where

$$\hat{J}_{m-1}(x,p,q,\eta,\zeta)=\sum_{i=1}^{I}\frac{a_i\gamma_i}{\pi}\int_{-\infty}^{\infty}\int_{-\infty}^{\infty}\hat{\imath}_{m-1}(x,p,q,\eta',\zeta')\times\exp\{-\gamma_i[(\eta-\eta')^2+(\zeta-\zeta')^2]\}d\eta'd\zeta'. \quad (17c)$$

The multiply scattered radiance penetrates the medium to a depth x_0 where it is backscattered. The backscattering phase function is also represented by a multi-Gaussian function

$$\tilde{\omega}\frac{\hat{P}(\pi-\Theta)}{4\pi}=\sum_{s=1}^{S}\mathcal{B}_s\exp\{-\epsilon_s[(\eta'+\eta)^2+(\zeta'+\zeta)^2]\}, \quad (18)$$

where

$$(\pi-\Theta)^2=(\eta'+\eta)^2+(\zeta'+\zeta)^2.$$

Thus the radiance which is propagated back to the receiver, $\hat{\imath}_{m+1}$, is subjected to the boundary condition

$$\hat{\imath}_{m+1}(x_0,p,q,\eta,\zeta)=\sum_{s=1}^{S}\mathcal{B}_s\int_{-\infty}^{\infty}\int_{-\infty}^{\infty}\exp\{-\epsilon_s[(\eta'+\eta)^2+(\zeta'+\zeta)^2]\}\times\hat{\imath}_m(x_0,p,q,\eta',\zeta')d\eta'd\zeta'. \quad (19)$$

The backscattered radiance $\hat{\imath}_{m+n}(x,p,q,\eta,\zeta)$ must satisfy an equation similar in form to Eq. (16b). Thus the following Neumann solution can be found:

$$\hat{\imath}_2(x,p,q,\eta,\zeta)=\exp(-[1-j(\eta p+\zeta q)][x_0-x])\hat{\imath}_2(x_0,p,q,\eta,\zeta), \quad (20a)$$

$$\hat{\imath}_{m+1}(x,p,q,\eta,\zeta)=\exp(-[1-j(\eta p+\zeta q)/\sqrt{3}][x_0-x])\hat{\imath}_{m+1}(x_0,p,q,\eta,\zeta), \quad m>1, \quad (20b)$$

where $\hat{\imath}_{m+1}(x_0,p,q,\eta,\zeta)$ is defined by Eq. (19). It follows in general that

$$\hat{\imath}_{m+n}(x,p,q,\eta,\zeta)=\int_{x_0}^{x}\hat{J}_{m+n-1}(\tilde{x},p,q,\eta,\zeta)\times\exp\{-[1-j(\eta p+\zeta q)/\sqrt{3}][\tilde{x}-x]\}d\tilde{x}, \quad n>1, \quad (20c)$$

$$\hat{J}_{m+n-1}(x,p,q,\eta,\zeta)=\sum_{i=1}^{I}\frac{a_i\gamma_i}{\pi}\int_{-\infty}^{\infty}\int_{-\infty}^{\infty}\hat{\imath}_{m+n-1}(x,p,q,\eta',\zeta')\times\exp\{-\gamma_i[(\eta-\eta')^2+(\zeta-\zeta')^2]\}d\eta'd\zeta'. \quad (20d)$$

The quantity that is measured by the lidar receiver is

$$M_N=\sum_{m=1}^{N}\sum_{n=1}^{N}M_{m,n}\delta_{m,N+1-n}, \tag{21}$$

where the Kronecker delta function is defined in Eq. (9) and

$$M_{m,n}=\int_{-\infty}^{\infty}\int_{-\infty}^{\infty}\int_{-\infty}^{\infty}\int_{-\infty}^{\infty}\hat{\hat{I}}_{m+n}(0,y,z,\eta,\zeta)\times R_{m+n}(y,z,\eta,\zeta)dydzd\eta d\zeta. \tag{22}$$

The response of the receiver is

$$R_{m+n}(y,z,\eta,\zeta)=\begin{cases}\dfrac{1}{\pi\psi^2}\delta(H\eta+y)\delta(H\zeta+z), & m+n=2,\ \eta^2+\zeta^2<\psi^2\\ 0, & m+n=2,\ \eta^2+\zeta^2>\psi^2\\ \dfrac{1}{3\pi\psi^2}\delta(H\eta+\sqrt{3}\langle y^2\rangle^{\frac{1}{2}})\delta(H\zeta+\sqrt{3}\langle z^2\rangle^{\frac{1}{2}}), & m+n>2,\ \eta^2+\zeta^2<3\psi^2\\ 0, & m+n>2,\ \eta^2+\zeta^2>3\psi^2\end{cases} \tag{23}$$

where the representation of R_{m+n} for $(m+n)=2$ and $(m+n)>2$ are related if the transformation in Eq. (14) is recalled. The receiver field of view half-angle is ψ, and H is the distance separating the lidar from the cloud boundary in units of optical depth (see Fig. 1).

Taking advantage of the Fourier integral convolution theorems renders it feasible to perform the integration in Eq. (22) by utilizing the appropriate Fourier transforms of $\hat{\hat{I}}_{m+n}$ and R_{m+n} (see Titchmarsh, 1948). The integration over angles can be performed analytically, as can the integration over p and q. However, integration over the various nested variables $\tilde{x}_l$ can only be performed numerically.

The evaluation of Eqs. (21) and (22) is simplified by the fact that

$$M_{m,N+1-m}:\ M_{1,N}=(N-1)!/(N-m)!(m-1)! \tag{24a}$$

Thus the summation in Eq. (21) can be replaced by a single term

$$M_N=2^{N-1}M_{1,N}. \tag{24b}$$

After some tedious analytical integration, one finds that

$$M_1=\begin{cases}\displaystyle\sum_{s=1}^{S}\frac{\mathcal{B}_s\exp(-2x_0)\delta[2(H'+x_0')-c\beta t']}{\pi\psi^2(H+x_0)^2} & (t'\geqslant 2H'/c\beta)\\ 0 & (t'<2H'/c\beta)\end{cases} \tag{25a}$$

$$M_N=\frac{2^{N-1}\exp(-2x_0)}{3\pi\psi^2}\delta[2(H'+x_0')-c\beta t']\times\sum_{i=1}^{I}\sum_{j=1}^{J}\cdots\sum_{(*)}\sum_{k=1}^{K}\sum_{s=1}^{S}\int_0^{x_0}\int_{\tilde{x}_2}^{x_0}\int_{\tilde{x}_3}^{x_0}\cdots\int_{\tilde{x}_{N-1}}^{x_0}\frac{a_i\gamma_i a_j\gamma_j\cdots a_k\gamma_k\mathcal{B}_s[1-\exp(-3C^{(N)}_{i,j,\ldots,k,s}\psi^2)]\prod_{l=1}^{N-1}d\tilde{x}_l}{(A^{(1)}_s+\gamma_i)(A^{(2)}_{i,s}+\gamma_j)\cdots(A^{(N-1)}_{i,j,\ldots,k-1}+\gamma_k)C^{(N)}_{i,j,\ldots,k,s}D^{(N)}_{i,j,\ldots,k,s}} \tag{25b}$$

$(N>1)$** $(t'>2H'/c\beta)$.

$M_N=0 \quad (t'<2H'/c\beta)$

(*) The summation over indices on the forward Gaussian peaks goes to the $(N-1)$th sum characterized by an index k. (**) The integration is

$$\int_0^{x_0}\cdots d\tilde{x}_1 \quad \text{for} \quad N=2.$$

The quantities shown in Eq. (25b) are

$$A^{(1)}_s=\epsilon_s$$

$$A^{(l)}_{i,j,\ldots,l-1,s}=\gamma_{l-1}A^{(l-1)}_{i,j,\ldots,l-2,s}/(\gamma_{l-1}+A^{(l-1)}_{i,j,\ldots,l-2,s})$$

$$B^{(1)}_s=(\tilde{x}_1-x_0)/\sqrt{3}$$

$$B^{(l)}_{i,j,\ldots,l-1,s}=(\tilde{x}_l-\tilde{x}_{l-1})/\sqrt{3}+(\gamma_{l-1}B^{(l-1)}_{i,j,\ldots,l-2,s})/(\gamma_{l-1}+A^{(l-1)}_{i,j,\ldots,l-2,s})$$

$$B^{(N)}_{i,j,\ldots,k,s}=(H+\tilde{x}_{N-1})/\sqrt{3}-(\gamma_k B^{(N-1)}_{i,j,\ldots,k-1,s})/(\gamma_k+A^{(N-1)}_{i,j,\ldots,k-1,s})$$

$$C^{(N)}_{i,j,\ldots,k,s}=A^{(N)}_{i,j,\ldots,k,s}+B^{(N)^2}_{i,j,\ldots,k,s}/\mathrm{D}^{(N)}_{i,j,\ldots,k,s}$$

$$D^{(N)}_{i,j,\ldots,k,s}=B^{(1)^2}_s/(\gamma_i+A^{(1)}_s)+\cdots+B^{(N-1)^2}_{i,j,\ldots,k-1,s}/(\gamma_k+A^{(N-1)}_{i,j,\ldots,k-1,s})$$

where $l-1=k$, when $(l)=(N)$.

$$M_N=0 \quad (t'<2H'/c\beta).$$

Summing contributions due to all orders of multiple scattering yields the total signal measured by the

lidar, *viz.*

$$M_{\text{total}}=\sum_{N=1}^{\infty} M_N. \tag{26}$$

The time required to compute the Nth order return for phase functions represented by S Gaussian functions in the backward direction, I Gaussian function in the forward direction immediately following the backward scattering event, J Gaussian functions representing the phase function in the next forward scattering event, etc., to K Gaussian terms representing forward scattering prior to the escape of radiation from the medium is

$$T_N\alpha(4.5)^N S\cdot I\cdot J\cdots K. \tag{27}$$

Because of economic considerations, Neumann solutions were computed for $N\lesssim 7$. Although the contribution of successive orders of scattering may initially increase as a function of the scattering order N, the contributions of the higher orders of scattering ultimately diminish as N increases. For the optical depths considered ($x_0\lesssim 6$) it was found that

$$\lim_{N\to N'} M_{N+1}/M_N\approx f, \tag{28}$$

where $3\lesssim N'<7$. Thus the higher orders of scattering can be represented by a geometric progression and

$$M_{\text{total}}\lesssim\sum_{N=1}^{7} M_N+fM_7/(1-f). \tag{29}$$

The equation for singly scattered returns is widely used by investigators who probe the atmosphere with lidar (see Derr, 1972). The energy which is backscattered by a single event is proportional but not equal to the expression for M_1 given by Eq. (25a). By presenting numerical results in terms of ratios taken with respect to M_1 one obtains quantities which are independent of the receiver telescope area, the receiver photoelectric efficiency and the transmitted energy. Furthermore, singly scattered lidar returns decrease rapidly as they emerge from greater optical depths within turbid atmospheres; much of this variation can be removed by presenting data as ratios of multiply scattered lidar returns to singly backscattered returns. The ratio M_2/M_1 is of special interest because it is frequently the most significant contribution to a multiply scattered return and because Eloranta (1972) has presented independent computations of this quantity. Ratios of higher order scattering to single scattering were found by Kunkel (1974) in his Monte Carlo investigations (see Kunkel and Weinman, 1976).

A convenient representation of the total multiply scattered energy returned to a lidar receiver is provided by the mean extinction correction factor $\bar{F}(x_0)$ which

TABLE 1a. Comparison between approximate Gaussian $\hat{P}(\Theta)/4\pi$ and actual phase functions $P(\Theta)/4\pi$ for nimbostratus cloud at $\lambda = 0.7$ μm (Kunkel, 1974).

Θ (deg)	$\frac{P(\Theta)}{4\pi}$	$\frac{\hat{P}(\Theta)}{4\pi}\left[\begin{matrix}I=3\\S=2\end{matrix}\right]$
0	1130	1080
0.5	550	568
1.0	92	99
1.5	21	20
2.0	8.9	9.6
3.0	3.1	2.9
4.0	1.7	1.8
5.0	1.2	1.3
175	0.009	0.009
176	0.011	0.011
177	0.013	0.013
178	0.018	0.018
178.5	0.025	0.024
179	0.028	0.031
180	0.043	0.041

is defined by

$$\bar{F}(x_0)=\frac{1}{2x_0}\ln\left(\frac{M_{\text{total}}}{M_1}\right). \tag{30}$$

The quantity M_{total} is given by Eqs. (25) and (26). Kunkel presents the results of his Monte Carlo analysis in terms of $\bar{F}(x_0)$; comparison of results obtained from the present analyses and the Monte Carlo technique is thus feasible.

3. Numerical results

The analysis which has been described requires that the phase function be approximated at forward and backward scattering angles by series of Gaussian functions [see Eqs. (7) and (18)]. Tables 1–3 present comparisons between exact and approximate phase functions and the parameters a_i, γ_i, $\mathfrak{G}_s$ and ϵ_s which are employed in the Gaussian approximations. It is evident that the Gaussian approximations become more accurate as the number of terms increase; however, Eq. (27) shows that the cost of performing the computations increases. The approximate C-1 cloud phase function shown in Table 2 with $S=4$ and $I=3$ was used to account for the backward scattering and the first forward scattering event, and subsequent forward

TABLE 1b. Parameters employed in the Gaussian approximation to the nimbostratus phase function.

$I=3$		$S=2$	
a_i	γ_i (rad^{-2})	$\mathfrak{G}_s$	ϵ_s (rad^{-2})
0.08	113	0.015	71
0.09	1480	0.026	1580
0.37	8860		

TABLE 2a. Comparison between approximate Gaussian $\hat{P}(\Theta)/4\pi$ and actual phase functions $P(\Theta)/4\pi$ for Cloud C-1 at $\lambda=0.7$ μm (Deirmendjian, 1969).

Θ (deg)	$\frac{P(\Theta)}{4\pi}$	$\frac{\hat{P}(\Theta)}{4\pi}\left[\begin{smallmatrix}I=2\\S=3\end{smallmatrix}\right]$	$\frac{\hat{P}(\Theta)}{4\pi}\left[\begin{smallmatrix}I=3\\S=4\end{smallmatrix}\right]$	
0	134	130	129	
1	94	94	94	
2	36	38	38	
3	10.6	10.3	10.4	
4	3.89	3.77	3.70	
5	2.13	2.25	2.20	
10	0.70	0.11	0.69	
15	0.47	0	0.51	
				Glory test*
165	0.012	0	0.012	0.012
170	0.015	0.004	0.014	0.014
175	0.027	0.027	0.025	0.025
176	0.035	0.030	0.029	0.029
177	0.030	0.032	0.031	0.031
178	0.033	0.031	0.031	0.030
179	0.034	0.034	0.034	0.028
180	0.051	0.050	0.051	0.027

* $\mathcal{B}_4=0$ for the test which removed the glory.

scattering events, $J, \ldots, K=2$, were described by the $I=2$ approximate phase function. The approximate C-1 cloud phase function with $S=3$ and $I, J, \ldots, K=2$ was used to describe all scattering events in the fog model.

The sequence of model ensembles from large to smaller scattering droplets are Ns, C-1 to Haze C. These models produce phase functions which become less peaked in the forward and backward directions. Scattering at small forward angles is most sensitive to particle size, but scattering at backward angles is sensitive to the size, shape and index of refraction of the scattering particles. The glory was removed from the C-1 phase function in the backward direction to illustrate the sensitivity of multiply scattered lidar returns to the details of the phase function at backward angles (see Table 2).

Results of the previously developed analysis are presented below. Ratios of various orders of scattering to single scattering and mean extinction correction factors are shown as a function of optical depth and receiver field of view for several turbid atmospheres. The parameters which characterize the cases under consideration are summarized in Table 4.

TABLE 2b. Parameters employed in the Gaussian approximation to the Cloud C-1 phase function.

$I=2$		$S=3$		$I=3$		$S=4$	
a_i	γ_i (rad^{-2})	$\mathcal{B}_s$	ϵ_s (rad^{-2})	a_i	γ_i (rad^{-2})	$\mathcal{B}_s$	ϵ_s (rad^{-2})
0.14	131	0.067	90	0.36	7.34	0.016	3.3
0.36	1100	−0.037	220	0.10	182	0.038	163
		0.020	5680	0.36	1090	−0.027	421
						0.024*	4320

* $\mathcal{B}_4=0$ for the test which removed the glory.

TABLE 3a. Comparison between approximate Gaussian $\hat{P}(\Theta)/4\pi$ and *actual* phase functions $\hat{P}(\Theta)/4\pi$ for Haze C at $\lambda=0.7$ μm (Deirmendjian, 1964).

Θ (deg)	$\frac{P(\Theta)}{4\pi}$	$\frac{\hat{P}(\Theta)}{4\pi}\left[\begin{smallmatrix}I=4\\S=3\end{smallmatrix}\right]$
0	2.50	2.48
5	1.90	1.93
10	1.20	1.18
15	0.80	0.81
20	0.60	0.59
25	0.40	0.41
155	0.013	0.013
160	0.013	0.013
165	0.014	0.014
170	0.014	0.014
175	0.013	0.013
180	0.016	0.016

A nimbostratus cloud model which was first considered by Plass and Kattawar (1971) was analyzed to yield the mean extinction correction factor $\bar{F}(x_0)$. The results of those computations are presented in Fig. 2. The results generally agree with those found by Kunkel (1974) from his Monte Carlo analysis. However, minor discrepancies appear at small optical depths which may be caused by narrow diffraction and glory peaks which tax the validity of the Gaussian approximation to the phase function. It should also be recalled that the values of $\bar{F}(x_0)$ exaggerate the differences between M_{total} for small x_0 because $\bar{F}(x_0)$ is inversely proportional to x_0.

Considering a cloud which contains smaller drops characterized by Deirmendjian's C-1 model provides results that may be compared to Eloranta's (1972) double-scattering analysis [see his Eqs. (4.67) and (5.3)]. Fig. 3 shows the ratio of double to single scattering computed by Eqs. (25a) and (25b) as a function of optical depth for several receiver fields of view. Fig. 4 shows the ratio of several orders of multiple scattering to single scattering for C-1 clouds when the receiver field of view is defined by $\psi=5$ mrad. Fig. 5 shows the mean extinction correction factor for this field of view. The results are compared with those obtained by Kunkel's Monte Carlo analysis.

The phase function of the Ns cloud is more strongly peaked in the forward direction than the C-1 cloud;

TABLE 3b. Parameters employed in the Gaussian approximation to the Haze C phase function.

$I=4$		$S=3$	
a_i	γ_i (rad^{-2})	$\mathcal{B}_s$	ϵ_s (rad^{-2})
0.52	0.08	0.014	0.58
0.49	1.9	−0.005	93
0.35	8.2	0.007	213
0.06	65		

TABLE 4. Summary of cases considered.*

Case	H' (km)	β (km^{-1})	ψ (rad)	Figure no.
Nimbostratus[a]	1	10	0.005	2
Cloud C-1[b]	1	10	0.001, 0.005, 0.010	3, 4, 5
Fog [Cloud C-1][b]	0.0125	10	0.005	6, 7
Haze C[c]	1	10	0.005, 0.030	8

* The scattering characteristics are appropriate for $\lambda = 0.7$ μm radiation.
[a] Kunkel (1974).
[b] Deirmendjian (1969).
[c] Deirmendjian (1964).

more multiply scattered light thus remains in the receiver field of view in the former case. Comparisons of Figs. 2 and 5 indeed shows that $\bar{F}(x_0)$ is larger for the Ns cloud than for the C-1 cloud. Looking ahead to the lower curve of Fig. 8 shows that $\bar{F}(x_0)$ continues to diminish as the phase function becomes less peaked in the forward direction in model Haze C.

The sensitivity of the multiple scattering correction factor to the phase function at backward angles is evident from a comparison of the solid and dashed curves in Fig. 5. The glory peak was removed from the approximate C-1 phase function to produce an artificial phase function which is also tabulated in Table 2. The $\bar{F}(x_0)$ corresponding to this artificial phase function is represented by the dashed curve of Fig. 5. The phase function has changed only for $178° \leqslant \Theta \leqslant 180°$; this reduces M_1 while higher scattering orders are reduced less as the scattering order increases. Eq. (30)

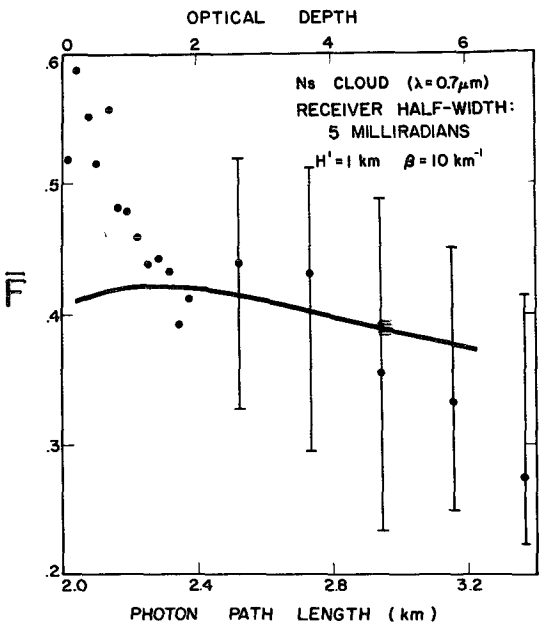

FIG. 2. Mean extinction correction factor $\bar{F}$ as a function of optical depth x_0 and total photon path length $2(H'+x_0')$ for a Ns cloud. The results obtained from the multi-Gaussian Neumann solutions are shown by the continuous line; these results are compared with those found by Kunkel's Monte Carlo analysis (dots).

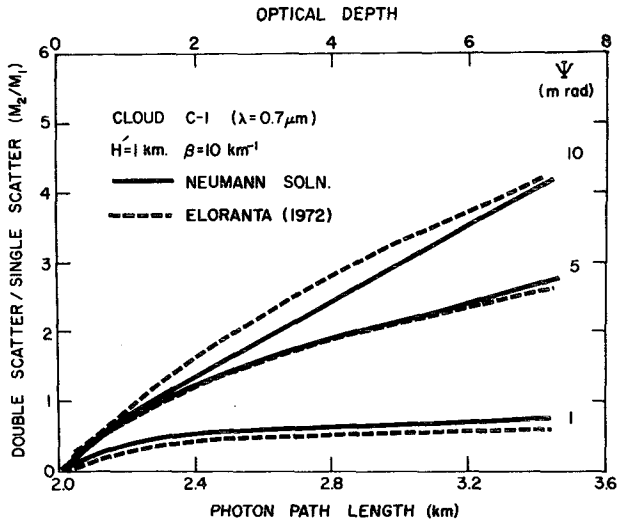

FIG. 3. Ratio of energy which is scattered twice to that which is singly scattered, M_2/M_1, as a function of optical depth x_0 and total photon path length $2(H'+x_0')$, for cloud C-1, 1 km from the lidar. The results of the Neumann solution are compared with those obtained from Eloranta's theory for several receiver fields of view.

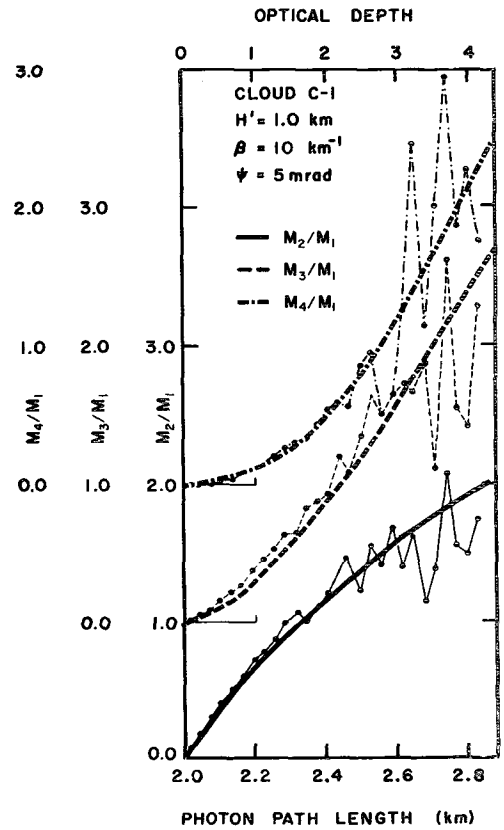

FIG. 4. As in Fig. 3 except for the ratio of multiply scattered energy to that which is singly scattered, M_N/M_1. The results are compared with those found by Kunkel's Monte Carlo analysis (dots).

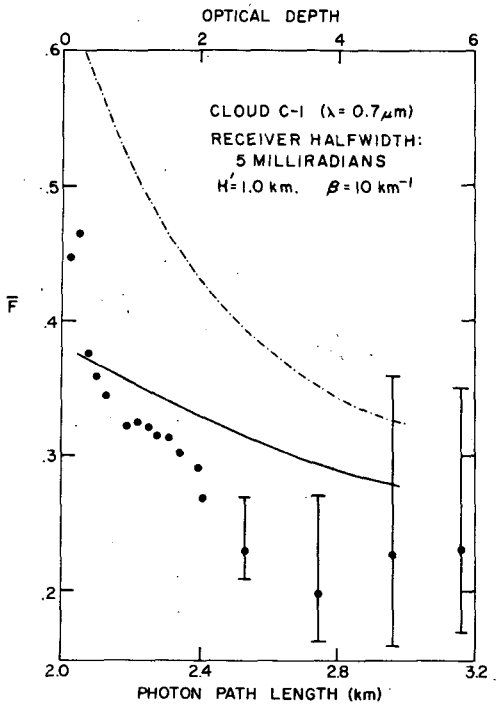

FIG. 5. Mean extinction correction factor $\bar{F}$ as a function of optical depth x_0 and total photon path length $2(H'+x_0')$, for cloud C-1. The results obtained from the multi-Gaussian Neumann solutions are shown as a continuous line and those of the Neumann solution which employed a phase function without a glory as a dot-dashed line. These results are compared with those found by Kunkel's Monte Carlo analysis.

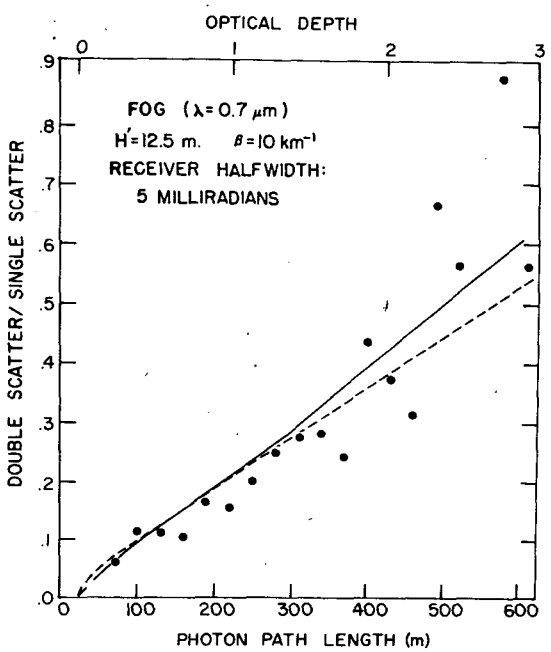

FIG. 6. As in Fig. 3 except for a fog model. The Neumann results are compared with those found by Kunkel's Monte Carlo analysis (dots) and Eloranta's theory (dashed line).

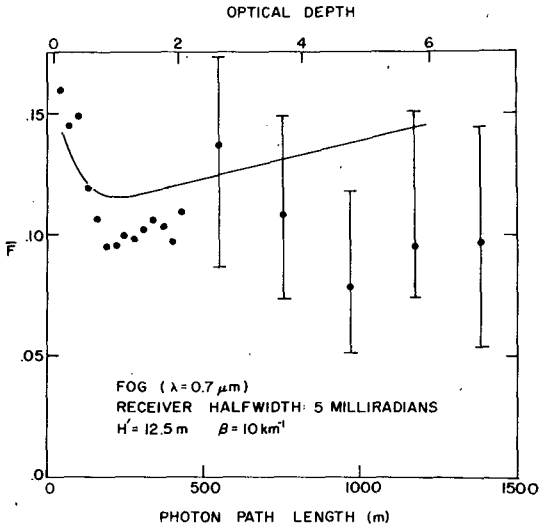

FIG. 7. As in Fig. 5 except for a fog model. The results are compared with those found by Kunkel's Monte Carlo analysis.

shows that a reduction in M_1 compared to M_{total} produces larger $\bar{F}(x_0)$ values.

The turbid atmospheres considered above were all located 1 km from the lidar. Placing the boundary of

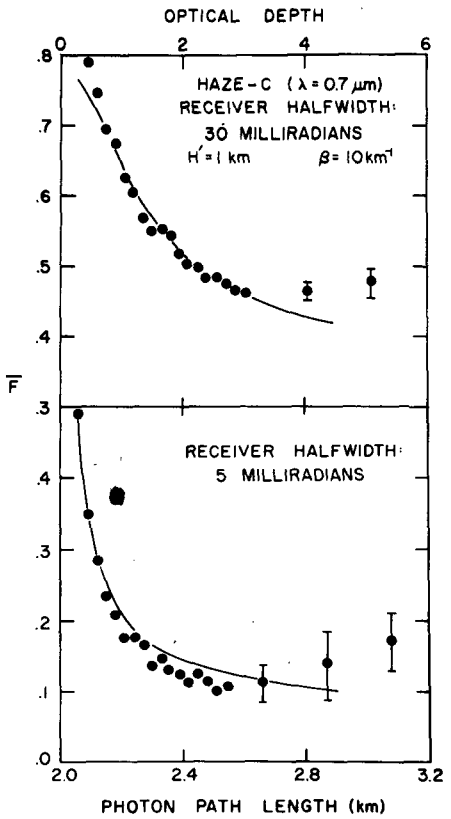

FIG. 8. As in Fig. 5 except for model Haze C. Results for $\psi = 30$ mrad and 5 mrad are shown in the upper and lower figures, respectively. The multi-Gaussian Neumann solutions are compared with those found by Kunkel's Monte Carlo analysis.

the cloud 12.5 m from the lidar simulates a fog. The receiver field of view is 5 mrad. The ratio of double to single scattering is presented as a function of optical depth in Fig. 6. The results are compared with those obtained by Eloranta and Kunkel. The mean extinction correction factor for this case is presented in Fig. 7. The results of Kunkel's Monte Carlo analysis are also shown. It is evident that the Neumann solution adequately describes the effect of multiple scattering for $x_0 \leqslant 6$. Reducing H' from 1 km to 0.0125 km appears to reduce the contribution of multiple scattering to lidar returns if all other parameters remain unchanged.

A Deirmendjian Haze C located 1 km from the lidar was another case previously considered by Plass and Kattawar. The parameters presented in Table 3 were used to approximate the haze phase function. The lower part of Fig. 8 shows the mean extinction correction factor as a function of optical depth for a receiver half-width angle, $\psi = 5$ mrad. The Neumann solution provides $\bar{F}(x_0)$ which agree with those found independently by Kunkel and by Thomas (1976) who used Monte Carlo techniques.

If the receiver field of view is expanded from 5 to 30 mrad, then the $\bar{F}(x_0)$ shown in the upper part of Fig. 8 is obtained. In this case more energy can be returned to the receiver telescope and $\bar{F}(x_0)$ increases accordingly.

4. Conclusions

A derivation has been presented for a solution to the equation of radiative transfer that describes the light scattered backward from turbid atmospheres which have been illuminated by collimated light pulses, i.e., the monostatic lidar problem. The Neumann solution to this problem can be obtained from Eqs. (25a), (25b), (26) and (29).

Numerical examples are presented for several model atmospheres. It is evident that multiple scattering is significant if receiver fields of view are comparable to the width of the forward peak in the scattering phase function even for optically thin atmospheres. The Neumann solution is satisfactory provided that a sufficient number of scattering orders are considered. The cost of computing higher order scattering terms rises rapidly. In practice, lidar returns measured from great optical depths are quite noisy and consideration of six orders of scattering is frequently sufficient.

The Neumann solution is most reliable if the phase function which characterizes the turbid atmosphere can be well approximated by a few Gaussian functions. Criteria for defining optimally fitted multi-Gaussian approximations to the actual phase functions become somewhat subjective if an insufficient number of Gaussians are employed to represent the actual phase function. However, fewer parameters than those presented in Tables 1–3 may sometimes provide acceptable estimates of multiply scattered radiances at less cost.

The ray tracing analysis of double scattering of Eloranta and the Monte Carlo investigations of Kunkel are distinctly different techniques, yet they provide data which are reasonably consistent with the results of the Neumann solution.

Acknowledgments. I wish to thank Mr. Peter Guetter for his patient and excellent cooperation in developing the computer program used in this study. Dr. E. W. Eloranta and Mr. K. E. Kunkel provided the results of their analyses which provided an incentive for the development of the ideas presented in this study. I also wish to thank Dr. R. W. L. Thomas of E. G. & G. for sending me the results of his Monte Carlo analysis so that the validity of the Neumann solution could be determined. This work was supported mainly by NSF Grant GA-37906 and in part by NASA Contract NAS1-14136.

REFERENCES

Collins, D. G., and M. B. Wells, 1965: Monte Carlo codes for the study of light transport, Vols. 1 and 2. RRA-T54, Radiation Research Associates Inc., Fort Worth, Tex.

Derr, V. E., Ed., 1972: *Remote Sensing of the Troposphere.* U. S. Gov't. Printing Office, Washington, D. C. 20402. [order No. C55.602:T75]

Deirmendjian, D., 1964: Scattering and polarization properties of water clouds and hazes in the visible and infrared. *Appl. Opt.*, **3**, 187–196.

——, 1969: *Electromagnetic Scattering on Spherical Polydispersions.* American Elsevier, 187–196.

Eloranta, E. W., 1972: Calculation of doubly scattered lidar returns. Ph.D. thesis, University of Wisconsin, Madison, 115 pp.

Kunkel, K. E., 1974: Monte Carlo analysis of multiply scattered lidar returns. M. Sc. thesis., Dept. of Meteorology, University of Wisconsin, Madison, 91 pp.

——, and J. A. Weinman, 1976: Monte Carlo analysis of multiply scattered lidar returns. *J. Atmos. Sci.*, **33**, 1772–1781.

Plass, G. N., and G. W. Kattawar, 1971: Reflection of light pulses from clouds., *Appl. Opt.*, **10**, 2304–10.

Rybicki, G. B., 1971: The searchlight problem with isotropic scattering. *J. Quant. Spectrosc. Radiative Transfer*, **11**, 827–849.

Thomas, R. W. L., 1976: Private communication.

Titchmarsh, E. C., 1948: *Introduction to the Theory of Fourier Integrals.* Oxford University Press, 50–51.

Weinman, J. A., and S. T. Shipley, 1972: Effects of multiple scattering on laser pulses transmitted through clouds. *J. Geophys. Res.*, **77**, 7123–7128.

——, J. T. Twitty, S. R. Browning and B. M. Herman, 1975: Derivation of phase functions from multiply scattered sunlight transmitted through a hazy atmosphere. *J. Atmos. Sci.*, **32**, 577–583.